

Optical and loss spectra of SiC polytypes from *ab initio* calculations

B. Adolph, K. Tenelsen, V. I. Gavrilenko, and F. Bechstedt

Friedrich-Schiller-Universität, Institut für Festkörpertheorie und Theoretische Optik, Max-Wien-Platz 1, 07743 Jena, Germany

(Received 9 July 1996; revised manuscript received 24 September 1996)

Frequency-dependent dielectric functions are calculated for the hexagonal polytypes $2H$, $4H$, and $6H$ as well as the cubic modification $3C$ of silicon carbide. The calculations are based on the *ab initio* pseudopotential-plane-wave method and random-phase approximation. We find a remarkable redistribution of the optical absorption and related spectra as reflectivity and energy loss due to the variation of the crystal structure and polarization direction. The relation of spectra and underlying electronic structures as well as the influence of nonlocality and quasiparticle effects are discussed. The numerical results are compared with experimental data available. [S0163-1829(97)00103-3]

I. INTRODUCTION

Silicon carbide (SiC) occurs in about 200 polytypes.¹ The two most extreme polytypes are zinc blende ($3C$) with pure cubic (C) stacking of the Si-C double layers in the $[111]$ direction and wurtzite ($2H$) with pure hexagonal stacking in the $[0001]$ direction. The other hexagonal (H) and rhombohedral (R) polytypes, nH and nR , represent combinations of these stacking sequences with a periodicity of n double layers in the stacking direction.² It is well known that the polytypism is of strong influence on the physical and chemical properties. For example, the energy gaps and the location of the conduction-band minima in \mathbf{k} space vary with the crystal structure (cf. Ref. 3 and references therein). With a change of the indirect energy gap of about 1 eV between the $3C$ and $2H$ polytypes,^{4,5} SiC represents an extraordinary example for the polytype influence on the electronic structure.

Optical spectroscopy should make visible the drastic changes in the electronic properties with the polytype. Recent advances in crystal growth of SiC have allowed the study of the optical properties of different polytypes. A systematic investigation of the vacuum-ultraviolet reflectivity has been presented for $3C$, $4H$, $6H$, and $15R$ crystals.⁶ Previous reports of reflectivity,⁷ electroreflectivity,⁸ and spectroscopic ellipsometry⁹ were mainly restricted to the zinc blende polytype, $3C$ -SiC. Recent calculations⁶ of the reflectivity within the linear-muffin-tin-orbital method and the atomic-sphere approximation need a calibration of the absolute reflectivity to compare with the experimental data. Absorption spectra have been calculated using *ab initio* pseudopotentials but neglect the effect of their nonlocal contribution to the optical transition operator.¹⁰ In the past simplified physical descriptions such as the empirical pseudopotential method and the orthogonalized-plane wave method have been applied to $3C$ -SiC (Refs. 11,12) and $2H$ -SiC.¹²

In this work we calculate the optical and dielectric properties of the hexagonal $2H$ -, $4H$ -, and $6H$ -SiC polytypes and compare them with those for cubic $3C$ -SiC. The *ab initio* calculations start from the atomic and electronic structures obtained within the density-functional theory (DFT) and local-density approximation (LDA). The influence of nonlocality and quasiparticle effects is discussed. We present the frequency dependence of the dielectric tensors as well as of reflectivity and energy-loss functions. By means of the band

structures we give explanations for the shifts and splittings of peak structures in the dielectric functions with the polytype. Furthermore, we compare our results with the experimental data.

II. METHOD

In order to examine the optical and energy-loss properties of SiC polytypes we have first calculated the imaginary parts of the elements of the second-rank dielectric tensor $\epsilon_{\alpha\beta}(\omega)$ in the optical limit,¹³

$$\text{Im}\epsilon_{\alpha\beta}(\omega) = \frac{8\pi^2 e^2 \hbar^2}{V} \sum_{c,v} \sum_{\mathbf{k}} \frac{\langle c\mathbf{k} | v_{\alpha} | v\mathbf{k} \rangle \langle c\mathbf{k} | v_{\beta} | v\mathbf{k} \rangle^*}{[\epsilon_c(\mathbf{k}) - \epsilon_v(\mathbf{k})]^2} \times \delta[\epsilon_c(\mathbf{k}) - \epsilon_v(\mathbf{k}) - \hbar\omega]. \quad (1)$$

Herein the Bloch eigenfunction $|n\mathbf{k}\rangle$ belonging to a band index n ($n=c$ conduction bands, $n=v$ valence bands) and a wave vector \mathbf{k} in the first Brillouin zone (BZ) is related to a Kohn-Sham eigenvalue $\epsilon_n(\mathbf{k})$ of the DFT-LDA. V denotes the crystal volume. The velocity operator \mathbf{v} in the optical transition matrix elements is defined by the commutator of single-particle Hamiltonian and space operator. Its replacement by the momentum operator \mathbf{p}/m leads to the neglect of the influence of the nonlocal contributions due to the nonlocal pseudopotentials. For a detailed discussion the reader is referred to Ref. 13, where the effect is discussed for cubic semiconductors. The neglect of the nonlocality effects increases the average oscillator strength by 15%. A similar overestimation arises for the dielectric constants and the low-frequency reflectivity spectra. The collective plasmon peak in the energy loss spectra is shifted to higher energies by about 2...3 eV. For that reason all calculations are performed including nonlocal contributions. The real parts of the components of the dielectric tensor $\text{Re}\epsilon_{\alpha\beta}(\omega)$ are calculated from expression (1) by means of a Kramers-Kronig transformation. Then the reflectivity and energy loss function follow using Fresnel's formula for normal light incidence or definition. Expression (1) is taken within the independent-particle approximation. Local-field effects have been neglected. Consequently, the exchange-correlation kernel due to the partial treatment of these effects in the DFT-LDA band structure does not influence the spectrum.

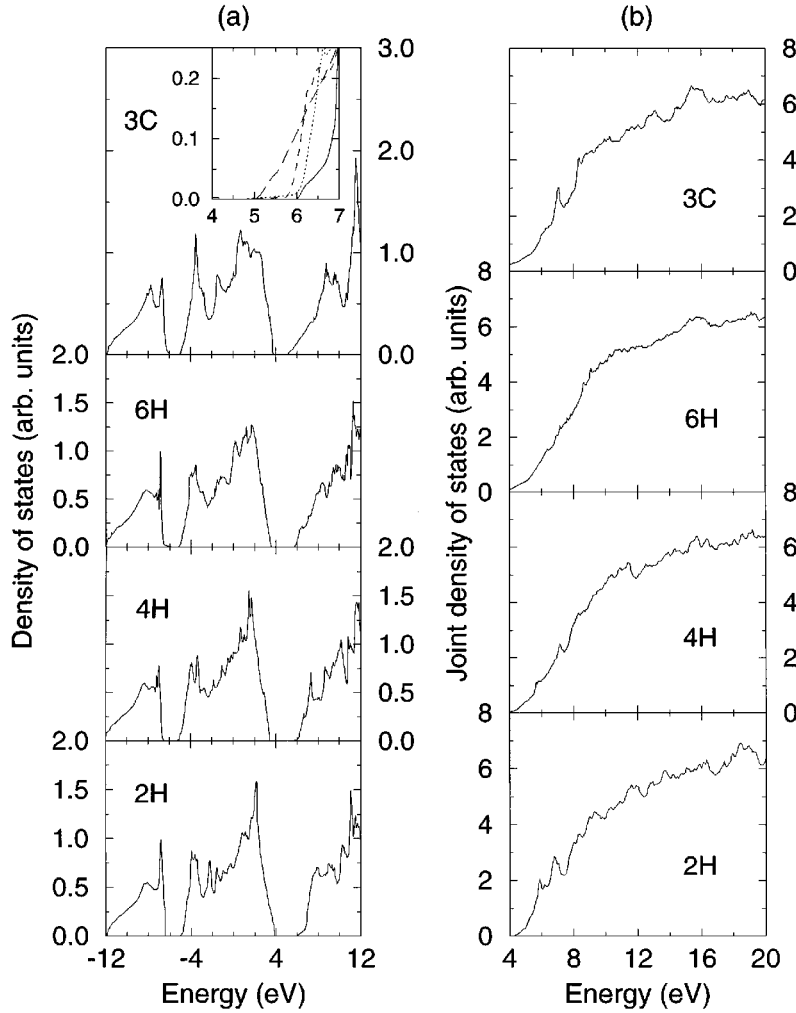


FIG. 1. Density of states (a) and joint density of states (b) for the $2H$, $4H$, $6H$, and $3C$ polytypes. The inset shows the lower edge of conduction bands. The energy zero in (a) corresponds to the tails of the pseudopotentials.

A crucial point in the calculations concern the \mathbf{k} -space integration. We use a linear tetrahedron method,¹⁴ based on 364 (231, 135, 231) \mathbf{k} points in the $\frac{1}{12}$ irreducible wedge of the BZ for $2H$ ($4H$, $6H$, $3C$) SiC. The density of the chosen meshes relates approximately to the magnitude of the corresponding BZ. In hexagonal Cartesian coordinates the dielectric tensor is diagonal with the nonzero elements ϵ_{xx} , ϵ_{yy} , and ϵ_{zz} . The \mathbf{k} -space integration for the two independent components ϵ_{\perp} and ϵ_{\parallel} may be restricted by constructing invariants $\epsilon_{\perp} = \frac{1}{2}(\epsilon_{xx} + \epsilon_{yy})$ and $\epsilon_{\parallel} = \epsilon_{zz}$ with respect to the point-group operations. The subscripts \perp and \parallel denote the direction of the electric-field vector of the incident light measured with respect to the c axis of the crystal. Throughout this paper the cubic $3C$ structure is treated within a hexagonal unit cell to make a direct comparison with the other polytypes possible. However, we average over the different Cartesian directions to avoid the small unphysical variations in the optical constants. In the band summation, 24 (48, 72, 36) conduction bands are included to get well-converged results for $2H$ ($4H$, $6H$, $3C$). The convergence with respect to the number of conduction bands is in particular a critical point for the calculation of the loss spectra, the main peaks of which occur at higher energies.

The underlying electronic structure is calculated within the DFT-LDA.¹⁵ The electron-ion interaction is treated by norm-conserving, *ab initio* pseudopotentials of the Bachelet-Hamann-Schlüter type¹⁶ in the fully separable Kleinman-

Bylander form.¹⁷ The electron wave functions are expanded in terms of plane waves up to an energy cutoff of 34 Ry. The restriction to the low cutoff arises from the use of softened carbon pseudopotentials.¹⁸ The lattice constants and the independent atomic coordinates are taken from total-energy minimization.² When quasiparticle corrections are discussed we refer to the recent calculation of the quasiparticle band structures for $2H$, $4H$, $6H$, and $3C$ (Ref. 3) and the method of their inclusion in the optical functions described in Ref. 13.

III. RESULTS

Before discussing the effect of the optical transition matrix elements, we consider the single-particle density of states [Fig. 1(a)] and the joint density of states [Fig. 1(b)]. Since the wave-vector dispersion of the quasiparticle corrections is not too big,³ the DFT-LDA data presented in Fig. 1 reflect the effect of the polytypism correctly, only the energies have to be shifted. The principal behavior of the density of states as well as the joint density of states is very similar for the four polytypes considered. The two peaks below the ionic gap exhibit a different behavior with the number n of Si-C bilayers in the unit cell. Whereas that at higher energy around -7 eV is rather independent of the polytype, the low-energy peak around -8 eV is broadened with rising number n . We relate this fact to the folding effect parallel to

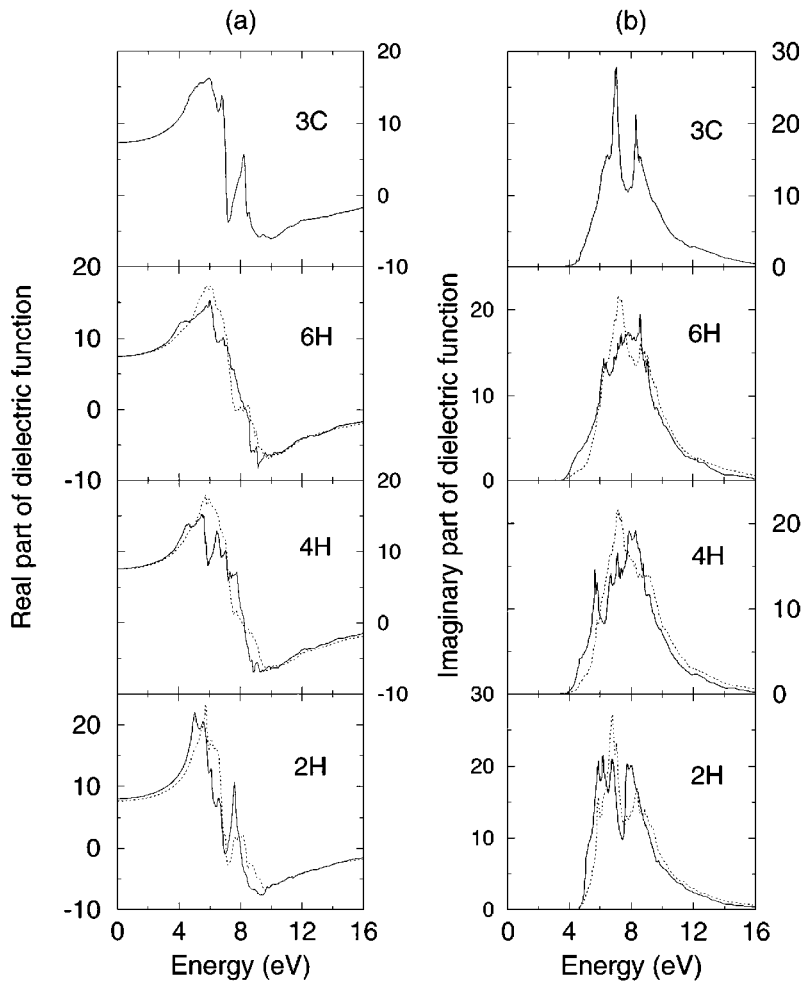


FIG. 2. Real (a) and imaginary (b) part of the dielectric tensor versus photon energy. Solid line: parallel component; dashed line: perpendicular component.

the c axis. It causes an opposite variation of the band curvature along the LM and HK lines in the hexagonal BZ.^{3,18} The intensity of the two most pronounced peaks at -3.5 and 2.1 eV in the region of the upper valence bands monotonically follow the hexagonality of the structures.² Strong contributions to these peaks also arise from the LM line. The most drastic change in the conduction-band region occurs near the onset of the density of states. Its steepness over several eV again follows the hexagonality of the polytype. The particular shape of the onset however depends on the number of bilayers and therefore on the folding effect as already has been pointed out by Lee *et al.*¹⁰ The consequences can be clearly seen in the joint density of states. Their low-energy tails increase with decreasing hexagonality. Consequently, the direct energy gap is the smallest in 3C-SiC (3.0 eV). The values for the other polytypes 6H, 4H, and 2H are 3.2, 3.5, and 3.9 eV. This direct gap is located at the M point in the hexagonal BZ.

Figure 2 shows the frequency dependence and the anisotropy of the dielectric function for the four polytypes under consideration. The small anisotropy effect in the 3C case due to the representation in a hexagonal cell and the use of a corresponding \mathbf{k} -point set for the BZ integration is not plotted. Rather the tensor components have been averaged. The spectra clearly show the interplay of matrix-element and density-of-states effects. This is more pronounced in the case of the imaginary parts. The parallel components are more strongly influenced by the polytypism than the perpendicular

components. This finding relates to the atomic structure which is in each bilayer essentially the same but differs due to the different stacking of the Si-C layers parallel to the c axis. The pronounced first peak of 3C around a photon energy of 7 eV with a shoulder at about 6.5 eV splits up into three (two) peaks for 2H (4H), while the peak intensities decrease remarkably. The tendency for the second peak in the 3C spectrum around 8.5 eV does not exhibit such a clear behavior. It however shows the same tendency as the first peak to shift to lower energies and to be broadened. This holds especially for 6H, where practically no pronounced peak structure exists any more. As a consequence of the band-structure folding only the small shoulders at the low- and high-energy sides are mentionable. In general, the folding effect seems to induce an effective smearing out of the peak structures as follows from the comparison of the spectra from 3C and 2H over 4H to 6H. It is therefore mainly related to the period of the translational symmetry in c -axis direction, but not to the relative number of twisted bonds, i.e., the hexagonality of the polytype.

The spectral behavior of the imaginary part of the perpendicular tensor components in Fig. 2(b) with hexagonality and cell size, i.e., folding, is in contrast to that of the parallel components. In general, for all polytypes two major peaks are observed with some fine structure. The energetical distance of the two-peak maxima vary with 1.5 . . . 2.0 eV only a little with the polytype. However, the double structure is redshifted for 3C and 2H against its position for 4H and

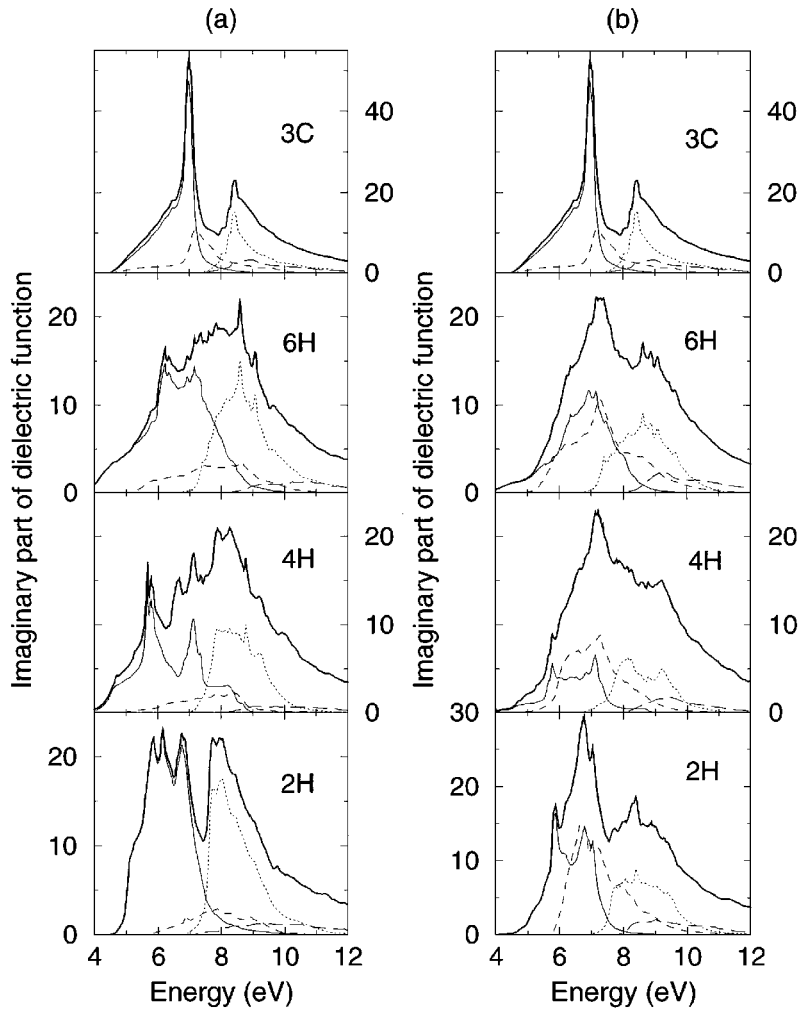


FIG. 3. Division of the spectra for $\text{Im } \varepsilon_{\parallel/\perp}(\omega)$ (solid line) into contributions related to transitions between groups of n upper valence bands and n lower conduction bands in a polytype with $2n$ atoms in the unit cell. Thin solid line: $v4n \rightarrow c1n$, dotted line: $v4n \rightarrow c2n$, short-dashed line: $v3n \rightarrow c1n$, and long-dashed line: $v3n \rightarrow c2n$. (a) Parallel component, (b) perpendicular component.

6H. The polytypes with more atoms in the unit cell, 6H and 4H, give again a rise to more broadened features and are rather again.

An exact relationship of electronic transitions and peaks occurring in the absorption spectrum is given for 3C-SiC in Ref. 13. Because of the larger number of bands such a detailed analysis is more complicated for the hexagonal polytypes and less helpful in the present stage of investigations. A preliminary discussion has been given in Ref. 11. As a striking feature we find for all hexagonal polytypes an enhanced absorption on the low-energy side of the spectra in the case of light polarization parallel to the c axis in agreement with Hemstreet *et al.*¹¹ and Lee *et al.*¹⁰ In the 2H this enhancement arises mainly from the transitions $\Gamma_{6v} \rightarrow \Gamma_{1c}$ and $K_{2v} \rightarrow K_{2c}$ around 5.1 and 6.1 eV in DFT-LDA. In 4H-SiC the peak at about 5.8 eV is much higher in the parallel case. It relates to transitions as $\Gamma_{6v} \rightarrow \Gamma_{1c}$ (5.55 eV), $K_{2v} \rightarrow K_{2c}$ (5.75 eV), $H_{3v} \rightarrow H_{3c}$ (5.68 eV), and $A_{5,6v} \rightarrow A_{1,3c}$ (5.91 eV). The pronounced tail with the steplike onset of the parallel 6H spectrum around 4 eV may be traced back to $L_{1,2,3,4v} \rightarrow L_{1,3c}$ transitions.¹⁰ For parallel polarization the $L_{4v} \rightarrow L_{1c}$ transition has an oscillator strength that is by a factor 4 larger than the oscillator strengths for $L_{4v} \rightarrow L_{3c}$ and $L_{3v} \rightarrow L_{1c}$ in the perpendicular case. Below this energy of about 4 eV the optical responses for the other polytypes 2H, 3C, and 4H are practically zero. This clearly reflects the behavior of the joint density of states.

A comparison of the analysis of contributions of certain optical transitions to the optical absorption is reasonable after summarizing the transitions into groups. Omitting the spin degeneracy, four valence bands have to be considered in the 3C case with two atoms per unit cell. According to the folding picture we consider groups of n bands for the nH structures. Such an analysis is represented in Fig. 3. We find that the low-energy tail and the lowest peaks are mainly related to transition between the $4n$ uppermost valence bands into the $1n$ lowermost conduction bands, where the group numbers 1, 2, 3, and 4 are energetically ordered. This finding holds especially for the parallel component of the dielectric tensor indicating the strong p_z -orbital character of the upper valence bands. In the lower $3n$ group of valence bands p orbitals in the plane perpendicular to the c axis dominate. In the perpendicular case the transitions between the lower $3n$ valence bands and the lowest $1n$ conduction bands plays an important role, especially for higher hexagonality. The high-energy peak structures are dominated by transitions between the highest $4n$ valence bands and the second group $2n$ of conduction bands. The transitions between $3n$ valence bands and $2n$ conduction bands occur at the high-energy sides of the spectra.

The most important trends with the crystal structure in the spectra of the real parts of the dielectric tensor follow already by discussing the low-frequency limit $\omega \rightarrow 0$, i.e., the tensor of electronic dielectric constants $\varepsilon_{\infty}^{\parallel/\perp} = \text{Re} \varepsilon_{\parallel/\perp}(0)$. The in-

TABLE I. Tensor of electronic dielectric constants for different polytypes of SiC. (* denotes that the values are calculated including local-field effects.)

Polytype hexagonality	2H		4H		6H		3C
	100%		50%		33%		0%
	$\epsilon_{\infty}^{\parallel}$	$\epsilon_{\infty}^{\perp}$	$\epsilon_{\infty}^{\parallel}$	$\epsilon_{\infty}^{\perp}$	$\epsilon_{\infty}^{\parallel}$	$\epsilon_{\infty}^{\perp}$	ϵ_{∞}
This work	8.02	7.64	7.61	7.54	7.49	7.48	7.33
Ref. 20	7.28	6.88	7.17	6.95	7.24	7.02	7.02
Ref. 21	7.32	6.91	7.20	6.96	7.24	7.00	6.95
Ref. 21*	6.69	6.38	6.65	6.47	6.70	6.53	6.33
Ref. 22	6.84	6.51	6.78	6.56	6.68	6.52	6.52
Ref. 23			6.70	6.50	6.55	6.50	6.38

clusion of the nonlocal contributions to the optical transition operator in the calculation brings the dielectric constants already close to the experimental values. The overestimation of about 15% . . . 20% is remarkably reduced.¹³ A further reduction results if local-field effects are included.¹⁹ In Table I the corresponding values are compared with those from other calculations^{20,21} or experiments.^{22,23} Independent of the complexity of the calculation or the experiment the parallel dielectric constant is larger than the perpendicular one for all hexagonal polytypes. The splitting between the two tensor components seems to increase with rising hexagonality. The same trend we find for the absolute values of the components. They increase with decreasing hexagonality, whereby the values of the parallel components differ much larger than the perpendicular ones. A word of caution is necessary concerning the accuracy of the DFT-LDA calculations. In our treatment $\epsilon_{\infty}^{\parallel/\perp}$ is derived as $\text{Re}\epsilon_{\parallel/\perp}(0)$ from a Kramers-Kronig transformation of $\text{Im}\epsilon_{\parallel/\perp}(\omega)$. The other DFT-LDA predictions estimate $\epsilon_{\infty}^{\parallel/\perp}$ directly by means of a special-point technique²¹ or from the density-functional perturbation theory.²⁰ Nevertheless, there is also a wide spread of experimental data. In the 6H case one finds besides $\epsilon_{\infty}^{\parallel}=6.68$ (6.55) and $\epsilon_{\infty}^{\perp}=6.52$ (6.50) from Ref. 22 (Ref. 23) also values $\epsilon_{\infty}^{\parallel}=6.49$ (8.18) and $\epsilon_{\infty}^{\perp}=6.17$ (5.16) depending on the fitting procedure.²⁴ Further work is needed here. For the application of different SiC polytypes in optical waveguides, e.g., of 3C and 4H or 6H, the differences in the refractive index numbers should be clarified.

The most important variations of the real part of the dielectric function [Fig. 2(a)] occur in the energy range between 6.0 and 9.0 eV. According to the double-peak structure in $\text{Im}\epsilon(\omega)$ for 3C the corresponding real part exhibits a clear two-oscillator behavior with three energy zeros. This character mainly disappears for 6H and 4H but remains in a weakened form for 2H. Consequently, we conclude again a remarkable influence of the size of the unit cell and the accompanying folded band structure, whereas the hexagonality has less influence. Due to the folding of the bands in \mathbf{k} space parallel to the c axis, there is a tendency for flattening the spectral features. In the energy range 7 . . . 8 eV the strongest anisotropies of the order of $\text{Re}[\epsilon_{\parallel}(\omega) - \epsilon_{\perp}(\omega)] \cong 10$ occur. They are mainly caused by the strong variation of the optical matrix elements. For the transitions into higher conduction bands near Γ that contribute significantly, the induced dipole

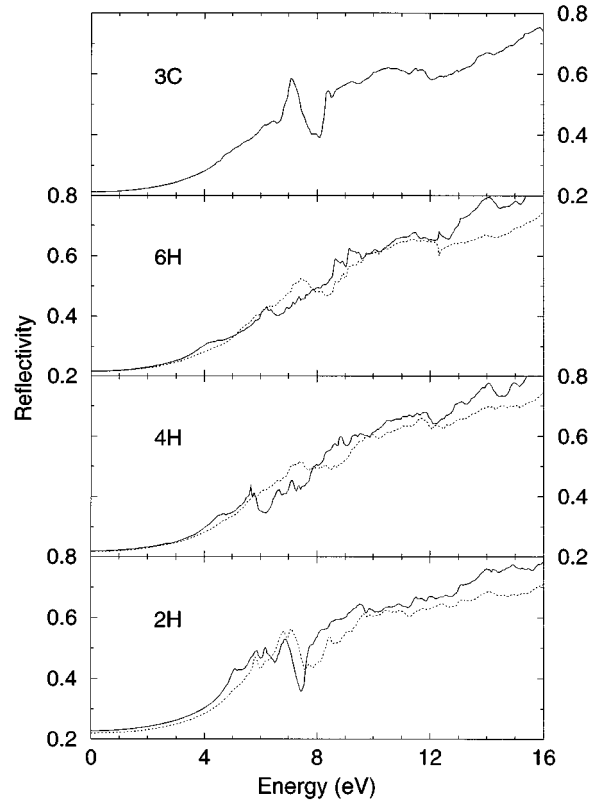


FIG. 4. Normal-incidence reflectivity for different polytypes and electric-field polarization parallel (solid line) and perpendicular (dotted line) to the c axis.

parallel to the c axis is much stronger than the perpendicular one.

The calculated real and imaginary parts of the dielectric tensor allow the calculation of important optical constants. The reflectivity spectra plotted in Fig. 4 are derived using the Fresnel formula for normal incidence assuming an orientation of the crystal surface parallel or perpendicular to the optical axis. Some tendencies described already for the dielectric functions occur in a less pronounced form. For a polarization with the electric field in the plane perpendicular to the c axis the polytype-induced reflectivity changes are smaller than for the opposite polarization. This could be a consequence of the fact that for that light polarization the optical response is less sensitive to the stacking of the Si-C bilayers. An oscillatorlike reflectivity behavior with a peak and a subsequent dip can be observed for the extreme cases 3C and 2H around photon energies of about 7 eV. For the 4H and 6H polytypes with intermediate hexagonalities but more extended unit cells this principal spectral shape is rather washed out as a consequence of the folding of the band structure in c direction. The folding effect also explains the appearance of several smaller structures in the reflectivity spectra in the energy interval between 5.5 and 9.5 eV. Above photon energies of 10 eV the influence of both the polytypism and the anisotropy is almost vanishing (except concerning the absolute values). The influence of the different averaged gaps disappears and the Drude behavior begins to develop.

In Fig. 5 the normal-incidence reflectivity calculated for light polarization in the plane perpendicular to the c axis is

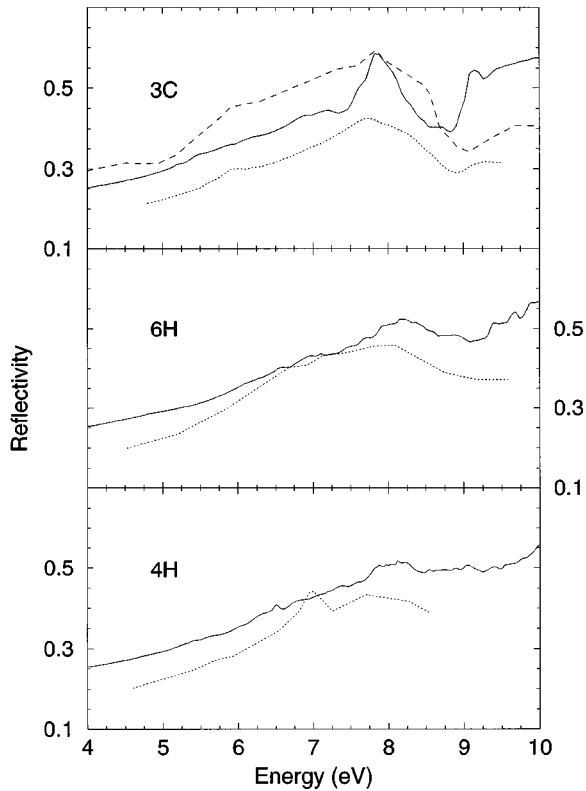


FIG. 5. Comparison of the calculated reflectivity versus photon energy (solid line) with experimental data (Ref. 6: dotted line, Ref. 7: dashed line) for normal incidence and light polarization in the plane perpendicular to the c axis.

compared with experimental spectra.^{6,7} To account for the excitation aspect not included in the DFT-LDA electronic structure the theoretical curves are shifted to higher energies by a constant value of 0.75 eV. The different aspects of such a scissors-operator approximation to remove the underestimation of the gaps in DFT-LDA have been discussed in a previous paper.¹³ The important point is that the value of the scissors operator is smaller than the quasiparticle shifts calculated for the various transitions.³ It nearly approaches half of the quasiparticle shift calculated for the indirect fundamental gaps. This fact seems to be general considering optical gaps in contrast to the case where these gaps are derived from photoemission and inverse photoemission.^{13,21} We believe that the need for reduction is a consequence of the electron-hole interaction (excitonic effects) omitted in the theoretical description but present in experiment. The measured principal spectral features are reproduced by the theory. This holds in particular for the peak close to 8 eV in the considered polytypes. It correlates with the high-energy peak in $\text{Im}\epsilon_{\perp}(\omega)$ [cf. Fig. 2(b)] and the first dip around 7.5 eV in $\text{Re}\epsilon_{\perp}(\omega)$ [cf. Fig. 2(a)]. This peak is most pronounced in the case of the 3C polytype and is somewhat smeared out for the hexagonal crystals 6H and 4H. The absolute values of the reflectivity are slightly overestimated compared with the experimental data given in Ref. 6 but not with first measurements of Wheeler.⁷ In the low-energy part we trace the discrepancy back to the overestimation of the high-frequency dielectric constant. Moreover, no lifetime and other (e.g., instrumental) broadening effects are included in the theoretical approach. The tendency for the overestimation of the

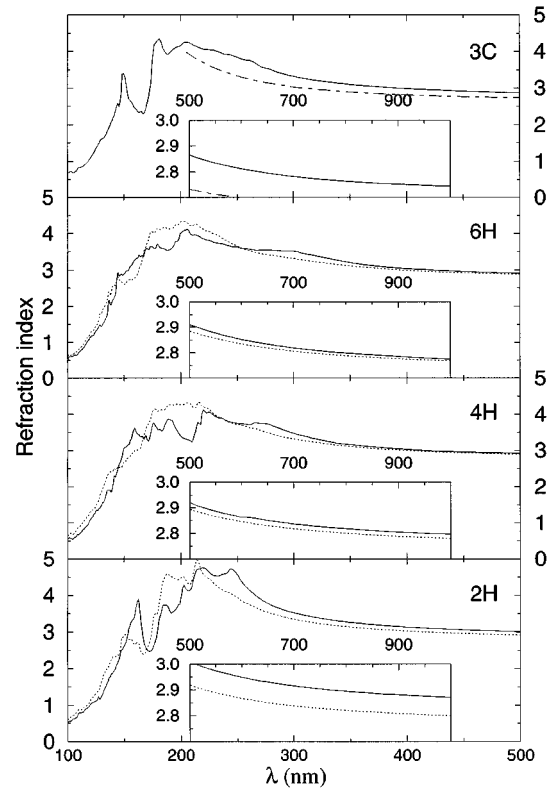


FIG. 6. Refractive index versus wavelength for light polarization parallel (solid line) and perpendicular (dotted line) to the c axis. The inset shows the long-wavelength region. Dot-dashed line: experimental data (Ref. 25).

reflectivity in the high-energy region is not only a consequence of the limited accuracy of the theoretical and numerical treatment. The sample quality, the surface treatment, the sample size, and technical difficulties of handling the vacuum UV radiation may influence the reflectivity spectra and therefore contribute to the discrepancy.

The knowledge of the complex dielectric tensors also allows the prediction of the frequency dependence of the real refractive index n . The spectra for light polarization parallel and perpendicular to the c axis of the polytypes are plotted in Fig. 6 versus the wavelength of the light in vacuum. In a wide range from the infrared to the blue spectral region the refractive index n represents the behavior of the high-frequency dielectric constant. The light polarized parallel to the c axis is more refracted than that with perpendicular polarization. This anisotropy of the hexagonal crystals decreases with the number n of Si-C bilayers in the unit cell. On average a nonlinear behavior versus the hexagonality is observed, indicating at least two opposite effects with rising hexagonality. In the ultraviolet range, for wavelengths below 250 nm, strong peaks already discussed in the case of the absorption spectra [Fig. 2(b)] and reflectivity (Fig. 4) appear. For 4H and 6H these peaks are slightly enhanced and become more pronounced than in the other spectra. Below 150 nm the Drude behavior of the valence electrons starts to develop. A nearly isotropic refractive index occurs with practically the same values for all polytypes. The quality of our calculations is indicated by the good agreement between theoretical and experimental refractive index in the case of 3C-SiC. The measurements are performed by means of spec-

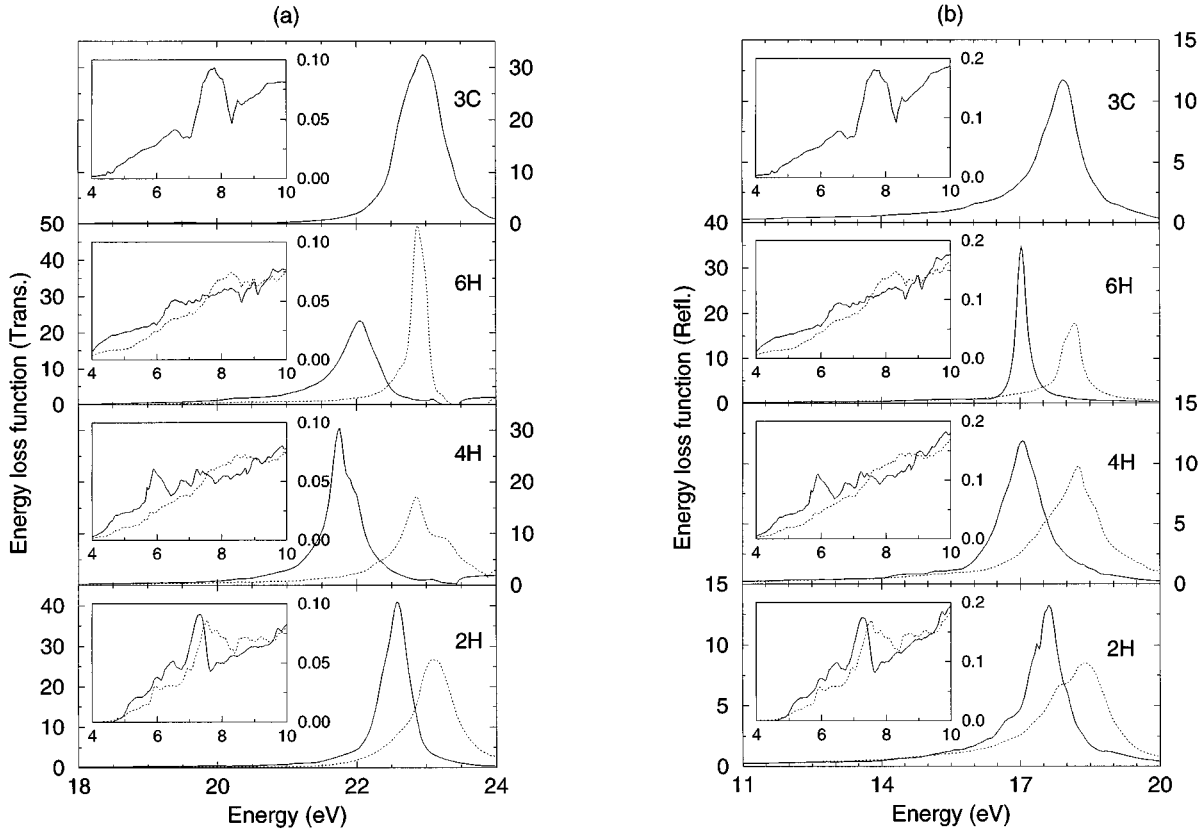


FIG. 7. Energy-loss function for transmission (a) and reflection (b) calculated from the parallel (solid line) and perpendicular (dotted line) components of the dielectric tensor.

troscopic ellipsometry for high-quality CVD layers.²⁵

Figures 7(a) and 7(b) represent energy-loss spectra for the scattering of low-energy electrons and light atoms. They are calculated according to $-\text{Im}[1/\varepsilon_{\parallel\perp}(\omega)]$ for particle transmission and $-\text{Im}[1/(\varepsilon_{\parallel\perp}(\omega) + 1)]$ for particle reflection and different orientations of the crystal with respect to the particle beam. Considering the energy loss functions around the main peak, i.e., for energies in the vicinity of the bulk or surface plasma frequency, where the collective action of the electrons dominates, we find the polytypism at least of the same importance as in the case of the optical properties. In the transmission case intensities of the functions derived from the parallel components of the dielectric tensor are nearly independent of the polytype, whereas the energetical positions of the parallel loss functions vary remarkably by about 1.5 eV. This variation shows again a parabolic behavior with the hexagonality. On the other hand, the positions of the main peaks of the loss functions derived from the perpendicular components coincide quite well. The latter ones differ only by about 0.3 eV, although an exact fixing of the peak maximum of the plasma peaks is not possible. We suggest using in the parallel situation the position of the main plasmon loss for the polytype identification by means of electron-energy-loss spectroscopy (EELS).

The absolute position of the center of the plasma peak is overestimated due to the neglect of quasiparticle and local-field effects. The value measured by means of EELS for 3C-SiC amounts to 22.1 eV.²⁶ We have to mention that the shape and the position of the plasma peak dramatically depends on the numerical details. Especially the convergence

with respect to the number of conduction bands is a crucial point. This is understandable from the fact that in the range of the plasma frequency both the real part and the imaginary part of the dielectric tensor become rather small. The two small quantities have to be calculated with a high precision for energies more than 20 eV above the valence-band maximum. A further problem arises from the band-structure calculation itself. It is expected²⁷ to lead to an underestimate of the oscillator strength for transitions into high-lying conduction bands. Nonlocality effects can by no means be omitted.

In fact, the influence of the crystal structure on the loss properties is not only clearly present for higher energies. In the range of the band-to-band transitions at lower energies we observe similar spectral features as already discussed in the case of the absorption. Practically the same features are observed in the loss functions in the reflection case [Fig. 7(b)]. However, due to the different background their intensity is lowered with respect to the transmission case [Fig. 7(a)]. The main peak in these loss spectra for transmission is found close to the surface plasmon. Its energy indeed follows the rule $\omega_{p\text{eff}}/\sqrt{2}$ as expected from the definition. However, we observe again a small overestimation by the theory.

IV. SUMMARY

In conclusion we have studied optical and dielectric properties of different polytypes of SiC using *ab initio* calculations. We have examined the density of states, the frequency-dependent dielectric tensors as well as related quantities like reflectivities and energy loss functions. Because of the sym-

metry in the hexagonal crystal lattice the dielectric tensor possesses two independent components. The accompanying anisotropy depends on the stacking of the Si-C bilayers, i.e., the hexagonality, and the sequence of this stacking, i.e., the extent of the unit cell parallel to the c axis of the crystal. Both effects influence the band structure and the optical transition matrix elements by changes of the third-nearest-neighbor or more-distant-neighbor interactions or the folding effect. Therefore, some spectral features vary monotonically with the hexagonality and are most pronounced in the case of the $2H$ polytype. Others are more important for the $4H$ and $6H$ crystals, which exhibit longer periods of the translational symmetry in c -axis direction. Whereas details of the band structure, as the crystal-field splitting, as well as integral quantities of the band structure, as the joint density of states follow a clear trend with the hexagonality of the polytype, such a monotonic behavior is not observed in the case of the optical properties. Rather, there is a near parabolic behavior versus the hexagonality due to the interplay of relative number of twisted bonds and length of the unit cell. The cubic $3C$ phase and the $2H$ wurtzite structure exhibit spectra quite different from those of the $4H$ and $6H$ polytypes with an intermediate hexagonality. This holds especially for spectra, which are related to the component of the dielectric tensor parallel to the c axis of the hexagonal crystal. In the opposite case, where the electric-field vector of the light vibrates par-

allel to the plane of the bilayers the stacking is of minor influence.

A small overestimation of the absolute values holds for the dielectric constants calculated. Comparing the calculated reflectivity with experimental curves we found a good agreement concerning the general features of the spectra, whereas the intensity is overestimated by the theory again. To get better agreement with experiment one should take into account quasiparticle, local field, and, in particular, excitonic effects. For a wide wavelength range in the infrared and visible spectral region we predict a higher light refraction for the electric-field vector parallel to the c axis of the polytypes. The energy loss spectra calculated react rather sensitively to the details of the numerical approaches, in particular to the number of conduction bands. The inclusion of quasiparticle and, especially, spatial nonlocal effects turned out to strongly influence the energetical positions of the loss spectra, leading to better agreement between theory and experiment.

ACKNOWLEDGMENTS

We thank P. Käckell for help with the computer code and useful discussions. This work was financially supported by the Deutsche Forschungsgemeinschaft (SFB 196, Project No. A8) and the EC Programme Human Capital and Mobility (Contract No. ERBCHRXCT 930337).

-
- ¹N.W. Jepps and T. Page, in *Progress in Crystal Growth and Characterization*, edited by P. Krishna (Pergamon Press, Oxford, 1983).
- ²P. Käckell, B. Wenzien, and F. Bechstedt, *Phys. Rev. B* **50**, 17 039 (1994).
- ³B. Wenzien, P. Käckell, F. Bechstedt, and G. Cappellini, *Phys. Rev. B* **52**, 10 897 (1995).
- ⁴W.J. Choyke, D.R. Hamilton, and L. Patrick, *Phys. Rev.* **133**, 1163 (1964).
- ⁵L. Patrick, D.R. Hamilton, and W.J. Choyke, *Phys. Rev.* **143**, 526 (1966).
- ⁶W.R.L. Lambrecht, B. Segall, M. Yoganathan, W. Suttrop, R.P. Devaty, W.J. Choyke, J.A. Edmond, J.A. Powell, and M. Alouani, *Phys. Rev. B* **50**, 10 722 (1994); *Appl. Phys. Lett.* **63**, 2747 (1993).
- ⁷B.E. Wheeler, *Solid State Commun.* **4**, 173 (1966).
- ⁸V.I. Gavrilenko, S.I. Frolov, and N.I. Klyui, *Physica B* **185**, 394 (1993).
- ⁹S. Logothetidis, H.M. Polatoglou, J. Petalas, D. Fuchs, and R.L. Johnson, *Physica B* **185**, 389 (1993).
- ¹⁰Keun-Ho Lee, C.H. Park, Byoung-Ho Cheong, and K.J. Chang, *Solid State Commun.* **92**, 869 (1994).
- ¹¹L.A. Hemstreet and C.Y. Fong, in *Silicon Carbide - 1973*, edited by R.C. Marshall, J.W. Faust, and C.Y. Ryan (University of South Carolina Press, Columbia, SC, 1974), p. 284.
- ¹²F. Herman, J.P. Van Dyke, and R.L. Kortum, *Mater. Res. Bull.* **4**, 167 (1969).
- ¹³B. Adolph, V.I. Gavrilenko, K. Tenelsen, and F. Bechstedt, *Phys. Rev. B* **53**, 9797 (1996).
- ¹⁴D. Jepsen and O.K. Anderson, *Solid State Commun.* **9**, 1763 (1971); G. Lehmann and M. Taut, *Phys. Status Solidi* **54**, 469 (1972).
- ¹⁵R. Stumpf and M. Scheffler, *Comput. Phys. Commun.* **79**, 447 (1994).
- ¹⁶G.B. Bachelet, D.R. Hamann, and M. Schlüter, *Phys. Rev. B* **26**, 4199 (1982).
- ¹⁷L. Kleinman and D.M. Bylander, *Phys. Rev. Lett.* **48**, 1425 (1982).
- ¹⁸P. Käckell, B. Wenzien, and F. Bechstedt, *Phys. Rev. B* **50**, 10 761 (1994).
- ¹⁹V.I. Gavrilenko and F. Bechstedt, *Phys. Rev. B* (to be published).
- ²⁰K. Karch, F. Bechstedt, P. Pavone, and D. Strauch, *Phys. Rev. B* **53**, 13 400 (1996); K. Karch, P. Pavone, W. Wellenhofer, D. Strauch, and R. Rösler, *ibid.* **53**, 6071 (1996).
- ²¹J. Cheng, Z.H. Levine, and J.W. Wilkins, *Phys. Rev. B* **50**, 11 514 (1994).
- ²²*Physics of Group IV Elements and III-V Compounds*, edited by K.-H. Hellwege and O. Madelung, Landolt-Börnstein, New Series, Group III, Vol. 17, Pt. a (Springer, Berlin, 1982).
- ²³H. Hobert and H. Dunken (private communication).
- ²⁴F. Engelbrecht and R. Helbig, *Phys. Rev. B* **48**, 15 698 (1993).
- ²⁵J. Heber and S. Karmann (unpublished).
- ²⁶B. Bartning, *Opt. Commun.* **4**, 78 (1971).
- ²⁷F. Aryasetiawan and O. Gunnarsson, *Phys. Rev. B* **49**, 7219 (1994).